Korean J. Chem. Eng., 35(5), 1108-1118 (2018)
DOI: 10.1007/s11814-018-0012-1

pISSN: 0256-1115
eISSN: 1975-7220

Application of copper sulfide nanoparticles loaded activated carbon for simultaneous adsorption of ternary dyes: Response surface methodology

Fatemeh Momtazan*, Azam Vafaei*,†, Mehrorang Ghaedi, Abdol Mohammad Ghaedi*, Daryoush Emadzadeh***,†, Woei-Jye Lau****, and Mohammad Mehdi Baneshi*****

*Chemistry Department, Gachsaran Branch, Islamic Azad University, Gachsaran 75818-63876, Iran
**Chemistry Department, Yasouj University, Yasouj 75914-35, Iran
***Department of Chemical Engineering, Gachsaran Branch, Islamic Azad University, Gachsaran, Iran
****Faculty of Chemical and Energy Engineering, Universiti Teknologi Malaysia, 81310 Skudai, Johor, Malaysia
*****Social Determinants of Health Research Center, Yasuj University of Medical Sciences, Yasuj, Iran
(*Received 3 August 2017 • accepted 2 February 2018*)

Abstract−Copper sulfide nanoparticles were synthesized and loaded on activated carbon (CuS-NPs-AC) for ternary dye removal. Fourier-transform infrared spectroscopy (FTIR), X-ray diffraction spectroscopy (XRD) and scanning electron microscopy (SEM) equipped with energy-dispersive X-ray spectroscopy (EDX) were used to characterize the synthesized materials. The performance of the materials was subsequently evaluated for simultaneous ultrasound assisted adsorption of Disulphine Blue (DB), Eosin Yellow (EY) and Safranin O (SO) dyes in ternary solution under different conditions that include variation in solution pH, initial concentrations of dyes, sonication time and adsorbent dosage. Response surface methodology (RSM) using central composite design (CCD) was employed to obtain the optimum experimental conditions. The maximum removal efficacies (88.39%, 68.49% and 55.69% for DB, EY and SO, respectively) were found at the optimum conditions: 3.63 min of sonication time, 0.02 g of CuS-NPs-AC, 7.76 mg L^{-1} of DB, 8.89 mg L^{-1} of EY, 9.87 mg L^{-1} of SO and pH 6.5. Very high adsorbent capacities of 198.12, 165.0, 139.58 mg g^{-1} for DB, EY and SO, respectively, were yielded from Langmuir isotherm as best fitted model. Kinetic study indicated that the pseudo-second-order kinetic model was well fitted to the experimental data of ternary adsorption process. The results of the study display very good adsorption efficiency of the synthesized adsorbent for dye removal with high adsorption capacity under optimum conditions.

Keywords: Adsorption, Central Composite Design, CuS-NPs-AC, Disulphine Blue, Eosin Yellow, Safranin O

INTRODUCTION

Wastewaters from many industries, such as paper, food, plastics, textile, antiseptics, cosmetics, and fungicides which use dyes for their products can contain dye pollutants at very low concentrations [1]. As dye possesses toxicity and carcinogenicity properties as well as longstanding environmental contaminant, it raises a great environmental concern with potential adverse effects to human health. Dye can enter into the human body through the digestive system via polluted food or water [2,3]. Therefore, it is necessary to remove it from wastewater before it enters into bodies of organisms [4]. Although a number of processes such as coagulation, precipitation, adsorption, electrochemical techniques, biosorption and ozonation are accessible for dye removal [5-8], adsorption in particular receives significant attention owing to its high efficiency, low operation cost and simple operation [9,10].

However, finding a new, yet effective, adsorbent for enhanced removal is very challenging. Among the adsorbent materials available, activated carbon (AC) that exhibits characteristics such as medium surface area, porous structure, middle adsorption capacities, fast adsorption kinetics can be used as support material for secondary nanomaterial embedment [11,12]. Some of the AC functional groups, namely -OH, -COOH, -C=O and NH_2, can potentially facilitate the loading of secondary nanoparticles on its surface, offering synergistic adsorption capacities for various species.

Our main purpose was to develop a modified physical adsorption method by depositing copper sulfide (CuS) nanoparticles [13] on the surface of AC. CuS is a nontoxic, low cost, easy available and high active site nanomaterial. The self-synthesized CuS was then used for selective and quantitative ultrasonic assisted removal of Disulphine Blue (DB), Eosin Yellow (EY) and Safranin O (SO) in ternary solution with high sorption capacities in short time. Influence of several important variables--sonication time, initial dyes concentration, amount of adsorbent and pH on the adsorption of selected dyes--was studied and optimized using central composite design (CCD). CCD, a statistical technique for planning, conducting, analyzing and interpreting data from experiments, is generally used to optimize and decide the factors influencing the performance of adsorption [14,15]. It decreases the number of experiments and minimizes error of experiments [16,17]. Our aim was also to study the adsorption kinetics and isotherms of dye removal using CuS loaded AC adsorbent for potential application in industry.

†To whom correspondence should be addressed.
E-mail: a.vafaei11@yahoo.com, D.emadzad@uottawa.ca

MATERIALS AND METHODS

1. Materials and Apparatus

Chemical reagents including copper (II) acetate hydrate, tri-sodium citrate, thioacetamide, ethanol, DB, EY, SO, acid chloride (HCl) and sodium hydroxide (NaOH) purchased from Merck (Dermasdat, Germany) were used without further purification. The solution pH was adjusted using HCl or NaOH and measured using pH/Ion meter (Model 827, Metrohm, Switzerland). The absorbance measurements used UV-Vis spectrophotometer (Lambda 25, Perkin-Elmer, USA). X-ray diffraction was recorded using diffractor (PW 1800, Philips, Netherlands) at 40 kV and 40 mA. The morphology of CuS was studied by scanning electron microscopy (KYKY-EM3200, KYKY, China) under an acceleration voltage of 26 kV. Ultrasonication was carried out in an ultrasonicator (Tecna 3, TECNO-GAZ) with a frequency of 5,060 kHz and at power of 250 W.

2. Synthesis of CuS-NPs-AC

CuS nanoparticles were prepared according to Ghaedi et al. [18]. At first, 10 mL of 0.1 mol L^{-1} copper (II) acetate hydrate ($Cu(CH_3COO)_2{\cdot}H_2O$) and 20 mL of 0.2 mol L^{-1} tri-sodium citrate were mixed in a 100 mL beaker. It was followed by adding 5 mL of 0.4 mol L^{-1} thioacetamide (CH_3CSNH_2) into the mixed solution slowly and continuous stirring for 1 h to allow CuS nanoparticles to grow slowly. Finally, the mixture was filtrated and the product (CuS) was washed several times with distilled water followed by drying at 80 °C for 15 h. To synthesize CuS-NPs-AC, nanoparticles and AC were mixed at 1 : 10 mass ratio under magnetic stirring [19,20]. 0.2 g of the prepared CuS was mixed with 2.0 g of AC before adding 200 mL ethanol. The mixture was further stirred for 20 h. The final solid material was filtered and washed several times by ethanol and distilled water before subjecting to heat treatment at 80 °C for 10 h.

3. Ultrasonic Assisted Adsorption Experiment

The ultrasonic assisted simultaneous adsorption of DB, EY and SO onto CuS-NPs-AC was carried out as follows: 50 mL ternary solution of DB, EY and SO at certain concentration (4-20 mg L^{-1}) according to the CCD matrix was prepared at corresponding pH (in the range of 5-9) by adjusting the solution using either 0.1 M HCl or 0.1 M NaOH and mixed completely with certain amount of CuS-NPs-AC (0.01-0.03 g). The mixture was then subject to sonication to achieve better dispersion of nanomaterials in the solution for greater adsorption rate. At last, 15 mL of sample was drawn out followed by immediate centrifugation. UV-vis spectrum of this sample was then recorded and DB, EY and SO content was calculated according to calibration curve obtained from derivative spectrophotometric method at 655, 483 and 412 nm, respectively. Fig. 1 shows the organic structure of three types of dyes used in this work. The amount of dyes adsorbed at equilibrium time, q_e (mg/g) and percentage dye removal efficiency, R (%) was calculated as follows [21]:

$$q_t = \frac{(C_0 - C_t)V}{M} \quad (1)$$

$$R = \frac{C_0 - C_t}{C_0} \times 100 \quad (2)$$

where, C_0 is the initial dyes concentration (mg/L), C_e is the concentration of dye at equlibrium time, V is the volume of solution (L) and M is the mass of adsorbent (g). Besides, to evaluate the regeneration performance of the adsorbent, the recovery process of dyes from the adsorbent was performed with 10 mL of a 0.5 M solution of nitric acid. For each cycle, the amount of adsorbent was kept constant (15 g). Before the adsorbent was reused for the following cycle, it was washed with excess 0.5 M nitric acid solution and distilled water followed by drying at 60 °C.

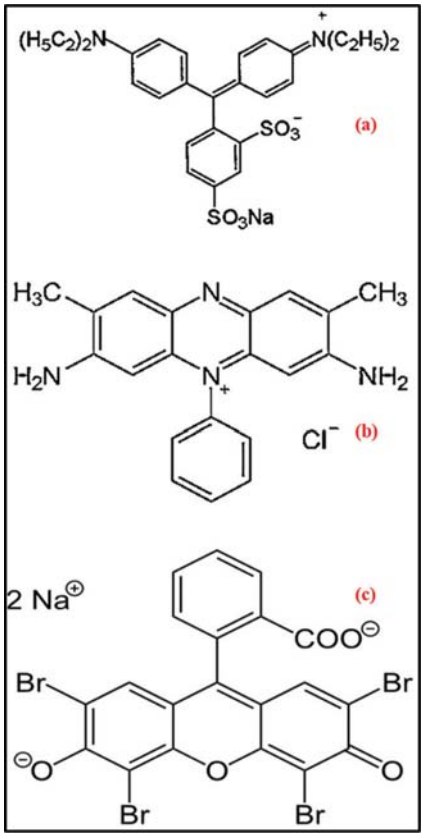

Fig. 1. Chemical structure of (a) DB, (b) SO and (c) EY.

4. Central Composite Design

The influence of effective variables on the adsorption efficiency like initial concentrations of DB, EY and SO (X_1, X_2 and X_3, respectively), pH (X_4), CuS-NPs-AC mass (X_5) and sonication time (X_6) was studied. CCD (using Design expert version 7.0 software) as a powerful experimental design technique for simultaneous optimization of parameters to increase the performance of adsorption process and to minimize error with minimum number of runs was used [21-23]. In this work, CCD matrix based on above parameters at five different levels (low, central, high, $+\alpha$ and $-\alpha$ as shown in Table 1) for 81 runs and their corresponding responses for each dye are presented in Table 2. Analysis of variance (ANOVA), desirability function approach, model summary statics such as coefficient of determination, adjusted R^2, predicated R^2 and Adeq. Precision, 3D surface plots, and the complete quadratic model for this 6-factor were studied as follows.

$$R\% = b_0 + \sum_{i=1}^{6} b_i x_i + \sum_{i=1}^{6} b_{ii} x_i^2 + \sum_{i=1}^{6} \sum_{j=i+1}^{6} b_{ij} x_i x_j, \quad (3)$$

Table 1. Experimental factors and levels in the central composite design

Factors	Levels				
	Low (−1)	Central (0)	High (+1)	$-\alpha$	$+\alpha$
X_1: Concentration of DB (mg L^{-1})	8	12	16	4	20
X_2: Concentration of EY (mg L^{-1})	8	12	16	4	20
X_3: Concentration of SO (mg L^{-1})	8	12	16	4	20
X_4: pH	6	7	8	5	9
X_5: CuS-NPs-AC mass (g)	0.015	0.020	0.025	0.010	0.030
X_6: Sonication time (min)	2	3	4	1	5

Table 2. The design matrix and the responses

Run	X_1	X_2	X_3	X_4	X_5	X_6	$R\%_{DB}$	$R\%_{EY}$	$R\%_{SO}$
1	12	4	12	7	0.02	3	71.23	45.12	28.69
2	16	16	8	8	0.015	2	62.39	42.69	31.20
3	12	12	20	7	0.02	3	79.65	39.25	39.65
4	12	12	12	7	0.02	1	75.28	76.95	63.25
5	8	8	16	6	0.025	2	76.32	41.20	32.58
6	8	8	16	8	0.025	2	72.89	39.65	25.36
7	16	8	8	6	0.015	4	68.25	35.68	38.25
8	8	16	16	6	0.025	4	81.20	45.12	41.23
9	8	16	8	8	0.015	4	73.69	39.12	37.56
10	8	8	16	6	0.015	4	74.91	48.69	42.36
11	12	12	12	7	0.03	3	82.56	51.23	45.96
12	16	8	8	6	0.015	2	85.69	38.96	41.25
13	8	16	8	8	0.015	2	62.35	45.35	34.69
14	16	16	16	6	0.015	2	68.25	51.36	30.23
15	8	8	8	6	0.025	2	82.66	71.36	54.28
16	8	8	8	8	0.015	4	69.25	48.96	34.69
17	16	8	16	6	0.015	2	81.23	31.25	27.53
18	16	16	16	8	0.025	4	63.25	56.28	68.39
19	8	16	8	8	0.025	2	71.25	63.28	42.58
20	8	8	8	8	0.025	2	67.89	61.28	31.28
21	8	16	8	6	0.015	4	85.69	45.36	37.96
22	8	16	16	6	0.015	2	61.23	49.38	31.25
23	16	8	16	8	0.015	2	81.25	31.25	26.85
24	16	16	8	8	0.025	4	63.25	52.96	45.36
25	16	8	16	6	0.025	4	72.69	47.69	44.25
26	12	12	12	7	0.02	3	91.23	75.69	61.39
27	12	20	12	7	0.02	3	61.23	52.36	33.62
28	8	16	16	8	0.015	2	65.89	41.25	31.23
29	12	12	12	7	0.02	3	91.36	75.69	62.69
30	16	8	8	8	0.025	2	71.69	55.23	35.62
31	20	12	12	7	0.02	3	81.26	68.69	55.36
32	16	8	16	8	0.025	2	82.69	42.36	34.25
33	16	16	16	6	0.025	4	62.35	45.39	44.56
34	16	16	8	8	0.015	4	55.39	31.25	28.69
35	16	16	8	6	0.025	4	80.23	51.26	39.65
36	16	16	16	6	0.025	2	68.56	55.36	41.26
37	16	8	8	8	0.025	4	62.39	58.60	38.56
38	16	8	8	6	0.025	4	81.23	55.62	41.23
39	12	12	12	5	0.02	3	92.36	65.38	55.26
40	8	16	8	6	0.025	2	85.36	75.36	55.35

Table 2. Continued

Run	X_1	X_2	X_3	X_4	X_5	X_6	$R\%_{DB}$	$R\%_{EY}$	$R\%_{SO}$
41	8	8	16	8	0.015	4	82.36	55.28	41.13
42	4	12	12	7	0.02	3	92.69	77.45	55.26
43	12	12	12	7	0.01	3	68.55	31.12	31.25
44	8	16	16	6	0.015	4	71.23	42.56	34.36
45	16	16	16	6	0.015	4	55.69	39.63	31.25
46	8	16	16	8	0.025	2	71.36	48.56	39.65
47	8	16	16	8	0.025	4	87.69	51.26	55.32
48	8	8	8	6	0.015	2	75.68	55.39	55.63
49	8	8	8	6	0.015	4	81.23	49.56	48.62
50	8	8	8	8	0.015	2	61.23	37.90	28.35
51	8	16	16	6	0.025	2	66.55	51.23	35.69
52	8	16	8	6	0.025	4	93.56	56.25	42.25
53	16	8	16	6	0.015	4	71.23	36.28	35.69
54	16	8	16	8	0.025	4	75.36	58.69	51.26
55	12	12	4	7	0.02	3	85.69	55.36	42.28
56	16	8	8	6	0.025	2	91.25	61.25	45.69
57	12	12	12	7	0.02	3	92.36	75.36	61.23
58	16	8	16	6	0.025	2	81.26	38.96	35.69
59	8	16	8	8	0.025	4	85.69	55.24	42.28
60	12	12	12	7	0.02	5	81.26	75.69	68.96
61	16	16	16	8	0.015	2	65.58	45.21	35.69
62	16	16	16	8	0.015	4	61.23	47.69	51.23
63	16	16	8	6	0.015	4	68.59	36.25	25.69
64	12	12	12	7	0.02	3	91.25	75.69	61.23
65	8	8	16	8	0.025	4	92.35	61.25	45.28
66	8	8	8	8	0.025	4	81.29	68.59	35.69
67	8	8	16	8	0.025	4	86.25	52.36	38.54
68	8	16	8	6	0.015	2	75.63	61.258	49.65
69	16	8	16	8	0.015	4	69.52	45.39	45.25
70	16	8	8	8	0.015	2	66.35	31.25	21.36
71	16	16	16	8	0.025	2	71.23	55.36	51.29
72	12	12	12	9	0.02	3	82.36	61.26	49.65
73	16	16	8	6	0.025	2	85.39	72.56	51.36
74	8	8	16	8	0.015	2	75.36	32.25	22.28
75	16	16	8	6	0.015	2	81.26	55.69	39.65
76	8	8	8	6	0.025	4	92.36	68.69	46.25
77	12	12	12	7	0.02	3	95.58	74.36	62.36
78	8	16	16	8	0.015	4	81.26	45.36	45.29
79	16	16	8	8	0.025	2	71.56	65.39	45.21
80	8	8	16	6	0.015	2	68.59	35.25	28.69
81	16	8	8	8	0.015	4	55.23	36.58	25.36

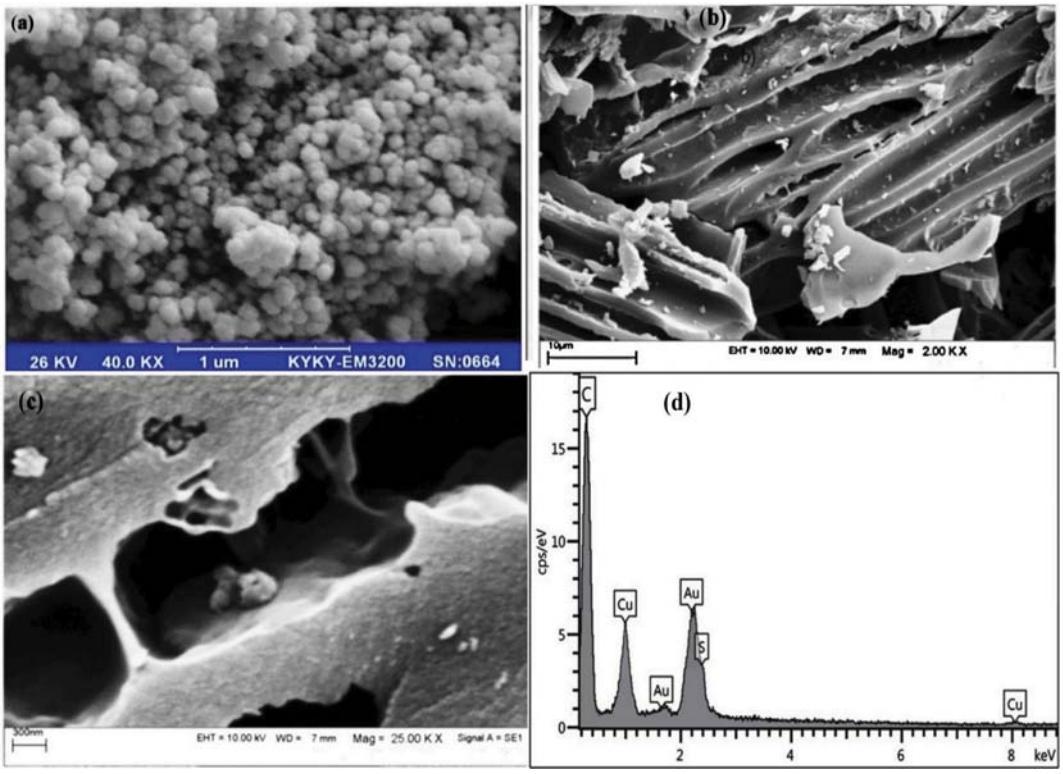

Fig. 2. (a) SEM image of CuS, (b), (c) SEM images of CuS-NPs-AC at different magnifications and (d) EDX spectra of CuS-NPs-AC.

where x_i's are the independent variables that are known for each experimental run. The parameter b_0 is the model constant; b_i's are the linear coefficients; b_{ii}'s are the quadratic coefficients and b_{ij}'s are the interaction coefficients [24,25].

RESULTS AND DISCUSSION

1. Characterization of Samples

The morphology of the CuS and CuS-NPs-AC was characterized with SEM and the results are shown in Figs. 2(a) and (b), respectively. The SEM image shows that the nanoparticles are well dispersed and stabilized over AC. It was found that the nanoparticles and their aggregation are grown in the spherical shapes with a relatively uniform in terms of shape and size distribution. According to the SEM images, the average size of CuS nanoparticles is estimated to be 20-100 nm. Fig. 2(c) shows the SEM image of the AC surface. By comparing the SEM images of the CuS-NP-AC with the AC surface, the deposition of CuS-NP strongly alters the homogeneous and relatively smooth surface of AC. To confirm the deposition of CuS nanoparticles on the surface of the AC, EDX analysis as shown in Fig. 2(d) was performed to indicate the existence of key elements: Cu, S and C in CuS-NPs-AC.

Fig. 3(a) presents the XRD pattern of the as-prepared CuS nanoparticles in the 2θ range of 15-80°. All the diffraction peaks at angle of 32.33° (101), 34.25° (102), 37.13° (103), 38.20° (006), 56.37° corresponding to the (110), 62.23° (108), and 70.20° (116) planes can be indexed to pure hexagonal covellite phase of CuS. The findings are in good agreement with the standard XRD pattern of the nanomaterial (JCPDS card No. 24-0060) [26,27]. The diffraction

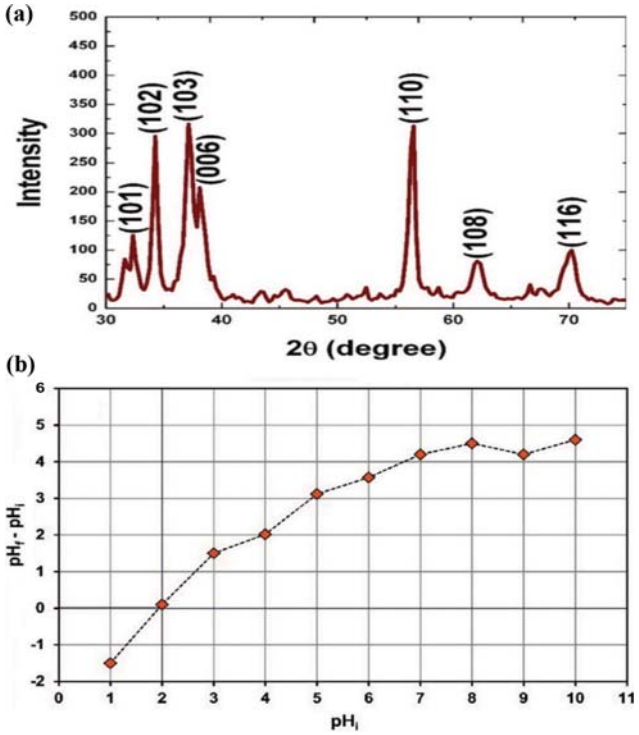

Fig. 3. (a) XRD pattern and (b) pH_f–pH_i vs. pH_i of the synthesized CuS-NPs-AC.

peaks due to $Cu(OH)_2$ and CuO in the XRD pattern could not be seen. The Debeye-Scherrer equation was used to evaluate the aver-

age nanocrystallite size (D).

$$D = \frac{0.9\lambda}{\beta \cos\theta} \quad (4)$$

where, D, λ, θ and β are the average crystal size in nm, the specific wavelength of X-ray used, the diffraction angle and the full-width half maxima (FWHM) of maximum peak intensity, respectively. The average size of the CuS nanoparticles was found to be about 40 nm.

Fig. 3(b) shows the zero point of charge (pH_{zpc}) of the CuS-NPs-AC. The pH_{zpc} of the CuS-NPs-AC was found to be 2.0. Thus, at the pH value below 2.0, the adsorbent surface charge is estimated to be positive. Consequently, columbic or electrostatic interactions do favor the adsorption of anionic dyes. Similar results have also been reported in other studies [19,20,28].

2. Spectral Characteristic of Ternary Mixture of Dyes

Absorbance spectra of DB, EY and SO dyes in single and ternary solutions (8 mg L^{-1}) as shown in Fig. 4(a) indicate strong spectra overlapping. Overlapping of spectra is not accurate in monitoring of the concentration of studied dyes at their maximum absorbance at respective maximum wavelength; thus, one useful method to solve the problem is based on derivative spectroscopy. Wavelength at all points in the spectrum of each dye is used to generate the first or higher derivative of spectral band absorbance. At proper wavelengths, a calibration curve is established and used for dye quantification. The values of correlation coefficient (R^2) are used to justify the efficiency and suitability of each wavelength. Therefore, first-order derivative of DB, EY and SO spectra in single and ternary solution is drawn and shown in Fig. 4(b). As can be seen at 655 nm, the first-order derivative of AO and EY spectrum is zero. Thus, at this wavelength the calibration curve is depicted ($R^2 \cong 1$) and used for DB quantification. Additionally, first-order derivative spectra of DB and EY found at wavelength of 412 nm are zero. Thus, at this wavelength the calibration curve is depicted ($R^2 \cong 1$) and used for SO quantification. Finally, the first-order derivative of spectra of DB and SO at wavelength of 483 nm is zero. Thus, at this wavelength the calibration curve is depicted ($R^2 \cong 1$) and used for EY quantification.

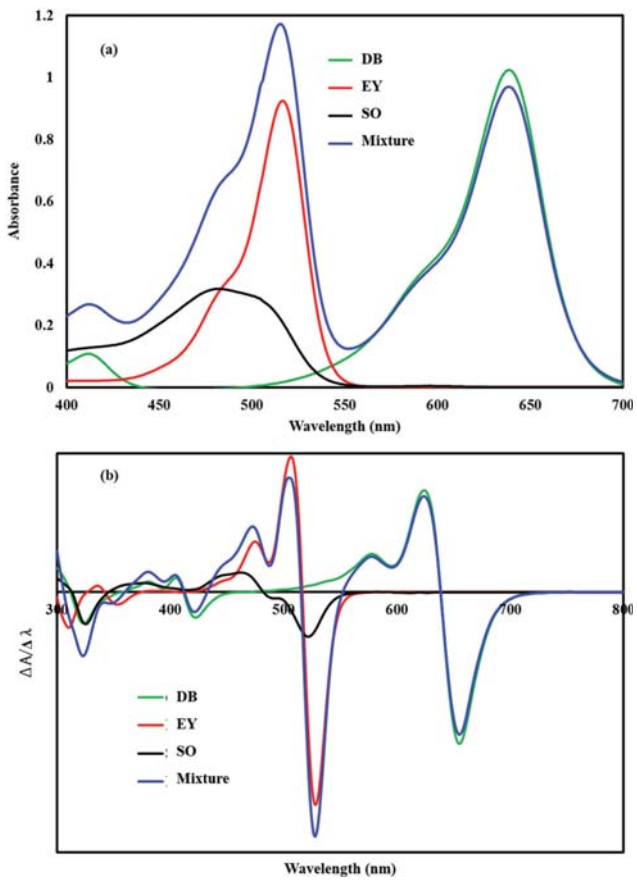

Fig. 4. (a) Absorption spectra of DB, SO and EY in single and ternary (mixture) solutions and (b) first order derivative spectra of DB, SO and EY in single and ternary (mixture) solutions.

3. Central Composite Design Analysis

ANOVA within 95% confidence interval for each response (Table 3) was applied. The results were based on p-value less than 0.0001 for each response and F-value of 112.927, 329.922 and 169.24 for DB, EY and SO dye, respectively, suggesting high efficiency of quadratic model for prediction of simultaneous adsorption of dyes process onto CuS-NPs-AC.

Additionally, p-value of 0.708, 0.063 and 0.067 for DB, EY and SO, respectively, confirmed that not-significant lack of fit is good and model is a fit for each response. Model summary included multiple correlation coefficient R^2 (0.9829, 0.9941 and 0.9885), adjusted R^2 (0.9742, 0.9911 and 0.9827), predicted R^2 (0.9602, 0.9846 and 0.9729) and adeq. precision (43.013, 66.739 and 55.265) for simultaneous removal of DB, EY and SO, respectively, further confirmed high efficiency of quadratic model for best predicting the performance of simultaneous dye adsorption. Based on variables with P-values lower than 0.05 an empirical relationship between the response and these variables was attained and expressed by the following second-order polynomial equations:

$$\begin{aligned} R\%_{DB} = {} & +91.96 - 2.80X_1 - 2.14X_2 - 0.84X_3 - 2.80X_4 + 3.39X_5 \\ & + 0.58X_6 - 1.44X_1X_2 + 0.17X_1X_3 - 1.06X_1X_4 - 0.65X_1X_5 \\ & - 5.15X_1X_6 - 2.33X_2X_3 + 0.66X_2X_6 + 4.45X_3X_4 - 0.97X_3X_5 \\ & + 0.48X_3X_6 + 0.73X_4X_6 + 0.88X_5X_6 - 1.12X_1^2 - 6.31X_2^2 \\ & - 2.20X_3^2 - 1.03X_4^2 - 3.98X_5^2 - 3.30X_6^2 \end{aligned} \quad (5)$$

$$\begin{aligned} R\%_{EY} = {} & +75.57 - 2.11X_1 + 1.42X_2 - 3.44X_3 - 0.83X_4 + 6.31X_5 \\ & + 1.73X_1X_2 + 1.71X_1X_3 + 0.90X_1X_4 + 0.92X_1X_5 \\ & - 0.98X_1X_6 + 0.92X_2X_3 - 0.69X_2X_4 - 0.80X_2X_5 \\ & - 4.08X_2X_5 + 2.22X_3X_4 - 2.95X_3X_5 + 3.02X_3X_6 + 0.94X_4X_5 \\ & + 2.56X_4X_6 - 0.69X_1^2 - 6.77X_2^2 - 7.13X_3^2 - 3.13X_4^2 - 8.67X_5^2 \end{aligned} \quad (6)$$

$$\begin{aligned} R\%_{SO} = {} & +62.15 + 1.78X_2 - 0.44X_3 - 0.98X_4 + 3.72X_5 + 1.98X_6 \\ & + 0.43X_1X_2 + 2.30X_1X_3 + 1.63X_1X_3 + 1.85X_1X_5 \\ & + 1.00X_2X_3 + 2.63X_2X_4 + 1.46X_2X_5 - 1.26X_2X_6 + 3.89X_3X_4 \\ & + 0.16X_1X_2 + 3.76X_3X_6 + 0.86X_4X_5 + 2.78X_4X_6 - 1.83X_1^2 \\ & - 7.87X_2^2 - 5.41X_3^2 - 2.54X_4^2 - 6.00X_5^2 + 0.87X_6^2 \end{aligned} \quad (7)$$

R% of each dye in range of CCD design level can be predicted using Eqs. (5)-(7) and the formula indicated good agreements between the experimental and predicted values of adsorption efficiency of studied dyes onto CuS-NPs-AC (see Fig. 5).

4. Effect of Variables as 3D Surface Plots

The response can be represented graphically, either in the 3D

Table 3. ANOVA for the response surface quadratic model of $R\%_{DB}$, $R\%_{EY}$ and $R\%_{SO}$

Source variation	DF[a]	$R\%_{DB}$				$R\%_{EY}$				$R\%_{SO}$			
		SS[b]	MS[c]	F-value	P-value	SS	MS	F-value	P-value	SS	MS	F-value	P-value
Model	27	8465.770	313.547	112.927	<0.0001	13741.800	508.956	329.922	<0.0001	9906.100	366.892	169.245	<0.0001
X_1	1	564.480	564.480	203.304	<0.0001	319.826	319.826	207.321	<0.0001	4.677	4.677	2.157	0.148
X_2	1	329.817	329.817	118.787	<0.0001	144.636	144.636	93.758	<0.0001	226.881	226.881	104.658	<0.0001
X_3	1	50.367	50.367	18.140	<0.0001	851.386	851.386	551.896	<0.0001	13.860	13.860	6.394	0.014
X_4	1	563.584	563.584	202.981	<0.0001	49.481	49.481	32.075	<0.0001	69.837	69.837	32.215	<0.0001
X_5	1	829.331	829.331	298.693	<0.0001	2869.440	2869.440	1860.060	<0.0001	995.695	995.695	459.306	<0.0001
X_6	1	24.477	24.477	8.816	0.00447	4.355	4.355	2.823	0.099	280.964	280.964	129.606	<0.0001
X_1X_2	1	132.595	132.595	47.756	<0.0001	192.557	192.557	124.822	<0.0001	11.637	11.637	5.368	0.024
X_1X_3	1	1.756	1.756	0.632	0.430	186.418	186.418	120.842	<0.0001	339.527	339.527	156.621	<0.0001
X_1X_4	1	72.548	72.548	26.129	<0.0001	51.531	51.531	33.404	<0.0001	170.205	170.205	78.514	<0.0001
X_1X_5	1	27.353	27.353	9.851	0.003	54.001	54.001	35.005	<0.0001	219.744	219.744	101.366	<0.0001
X_1X_6	1	1696.620	1696.620	611.055	<0.0001	61.215	61.215	39.682	<0.0001	1.479	1.479	0.682	0.412
X_2X_3	1	348.382	348.382	125.474	<0.0001	54.081	54.081	35.057	<0.0001	63.820	63.820	29.440	<0.0001
X_2X_4	1	10.579	10.579	3.810	0.056	30.371	30.371	19.688	<0.0001	442.208	442.208	203.987	<0.0001
X_2X_5	1	1.538	1.538	0.554	0.460	41.294	41.294	26.768	<0.0001	135.985	135.985	62.729	<0.0001
X_2X_6	1	27.931	27.931	10.060	0.002	1067.880	1067.880	692.237	<0.0001	101.581	101.581	46.859	<0.0001
X_3X_4	1	1268.250	1268.250	456.774	<0.0001	315.986	315.986	204.833	<0.0001	967.754	967.754	446.418	<0.0001
X_3X_5	1	59.985	59.985	21.604	<0.0001	558.330	558.330	361.927	<0.0001	1.642	1.642	0.757	0.388
X_3X_6	1	14.669	14.669	5.283	0.026	583.633	583.633	378.330	<0.0001	906.989	906.989	418.387	<0.0001
X_4X_5	1	1.363	1.363	0.491	0.487	56.415	56.415	36.570	<0.0001	46.803	46.803	21.590	<0.0001
X_4X_6	1	33.727	33.727	12.147	0.001	418.550	418.550	271.318	<0.0001	495.563	495.563	228.599	<0.0001
X_5X_6	1	49.773	49.773	17.926	<0.0001	1.922	1.922	1.246	0.269	0.374	0.374	0.172	0.680
X_1^2	1	40.310	40.310	14.518	0.000	15.308	15.308	9.923	0.003	106.844	106.844	49.286	<0.0001
X_2^2	1	1273.550	1273.550	458.685	<0.0001	1468.450	1468.450	951.895	<0.0001	1979.970	1979.970	913.345	<0.0001
X_3^2	1	154.685	154.685	55.711	<0.0001	1628.100	1628.100	1055.390	<0.0001	937.794	937.794	432.597	<0.0001
X_4^2	1	33.693	33.693	12.135	0.001	313.328	313.328	203.110	<0.0001	206.615	206.615	95.310	<0.0001
X_5^2	1	506.221	506.221	182.321	<0.0001	2402.850	2402.850	1557.600	<0.0001	1153.350	1153.350	532.030	<0.0001
X_6^2	1	348.187	348.187	125.403	<0.0001	0.467	0.467	0.303	0.584	24.304	24.304	11.211	0.002
Lack of fit	49	133.279	2.720	0.784	0.708	80.434	1.642	4.949	0.064	112.973	2.306	4.799	0.067
Pure error	4	13.880	3.470			1.330	0.330			1.920	0.480		
Cor total	80	8612.900				13823.500				10020.990			

[a]Degree freedom
[b]Sum of square
[c]Mean square

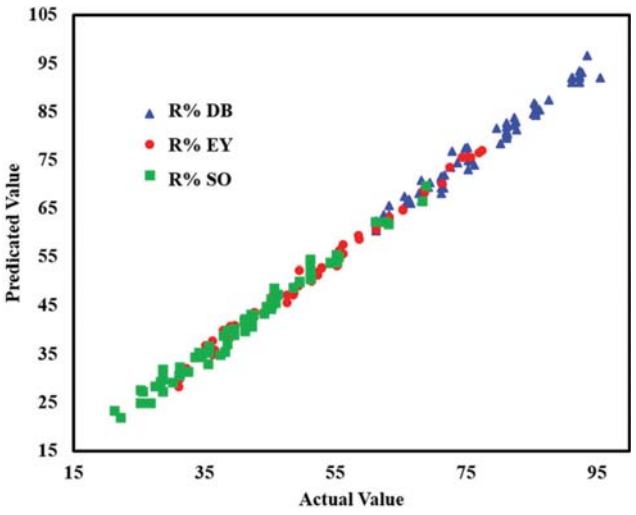

Fig. 5. The actual values versus the predicted data of normalized simultaneous removal of DB, SO and EY.

space or as contour plots that help visualize the shape of the response surface [29]. 3D response plots with contour background (see Fig. 6) are curves of constant response drawn in the x_i, x_j plane, keeping all other variables fixed in central levels so the interaction of the variables and the optimum level of each variable for maximum response could be determined.

The effect of initial dye concentration on removal percentage as shown in Fig. 6(a) and (c) reveals that removal efficiencies decrease by increasing the initial dye concentration. The removal efficiencies are promising until the system reaches its equilibrium condition. Once the CuS-NPs-AC is saturated, its efficiencies against dye removal are negatively affected, leading to lower dye separation rate.

On the other hand, the effect of sonication time on the SO adsorption as shown in Fig. 6(b) indicates that removal percentage of SO increases with increasing sonication time. The improved sorption values with increasing sonication time could be due to enhanced mass transfer of dye molecules from the bulk solution to the outer surface of adsorbent particles, causing higher probability of collision between the adsorbent and the absorbed particles. At higher sonication times, the active sites of the outer surface will be saturated and molecules of dye will be entranced into the adsorbent pores. The removal rate of dye molecules tends to decrease gradually once the adsorbent approaches its equilibrium conditions. Similar discussion can also be found elsewhere [30].

The effects of pH in the range of 5-9 on the DB adsorption as presented in Fig. 6(b) show that the removal percentage of DB is negatively affected at higher solution pH. To recognize the mechanism of adsorption, it is necessary to determine the pHzpc of the adsorbent. As can be seen from Fig. 3(d), a pHzpc of two is obtained for the adsorbent. Therefore, at the $pH>pH_{zpc}$, the surface of the adsorbent is negatively charged, creating higher electrostatic repulsive forces against the anionic dye. On the other hand, the presence of additional OH^- ions can compete with the anionic dye for the adsorption on the sites. These phenomena cause a decrease in

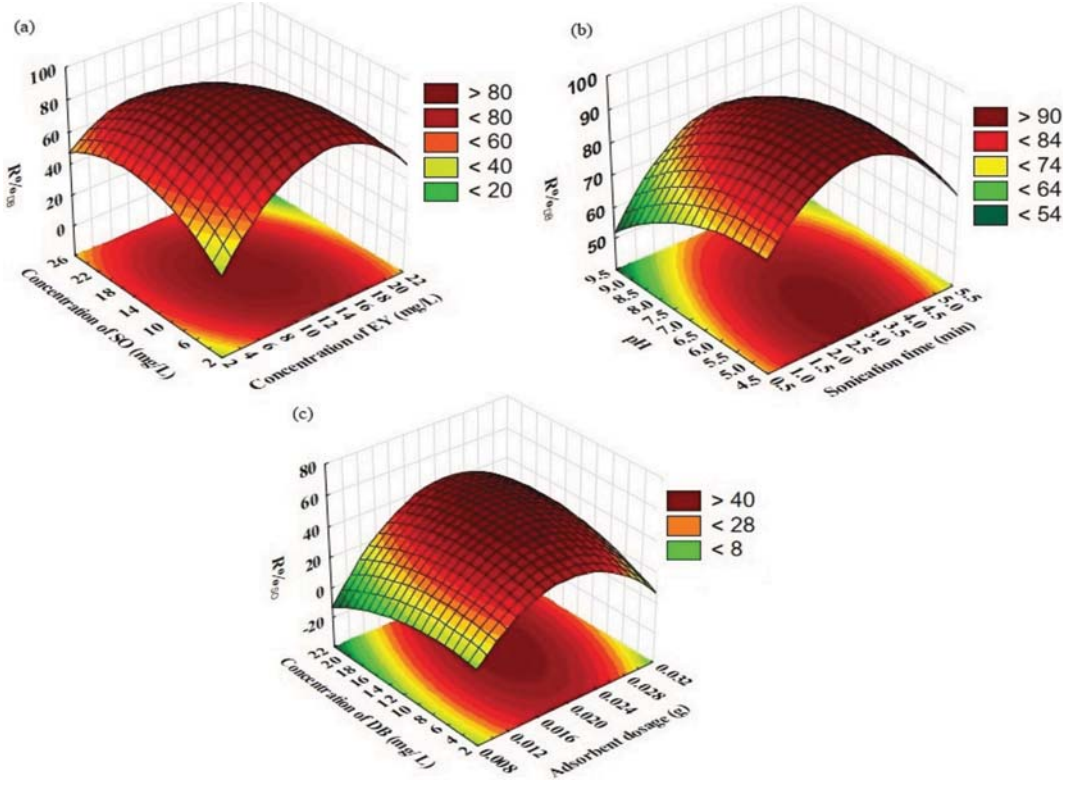

Fig. 6. 3D response surface plot, (a) concentration of SO and EY on DB dye removal, (b) pH and sonication time on DB dye removal and (c) concentration of DB and adsorbent dosage on SO dye removal (Conditions: Adsorbent dosage: 0.01-0.03 g; pH: 5-9; initial dye concentration: 4-20 mg L^{-1} and sonication time: 1-5 min).

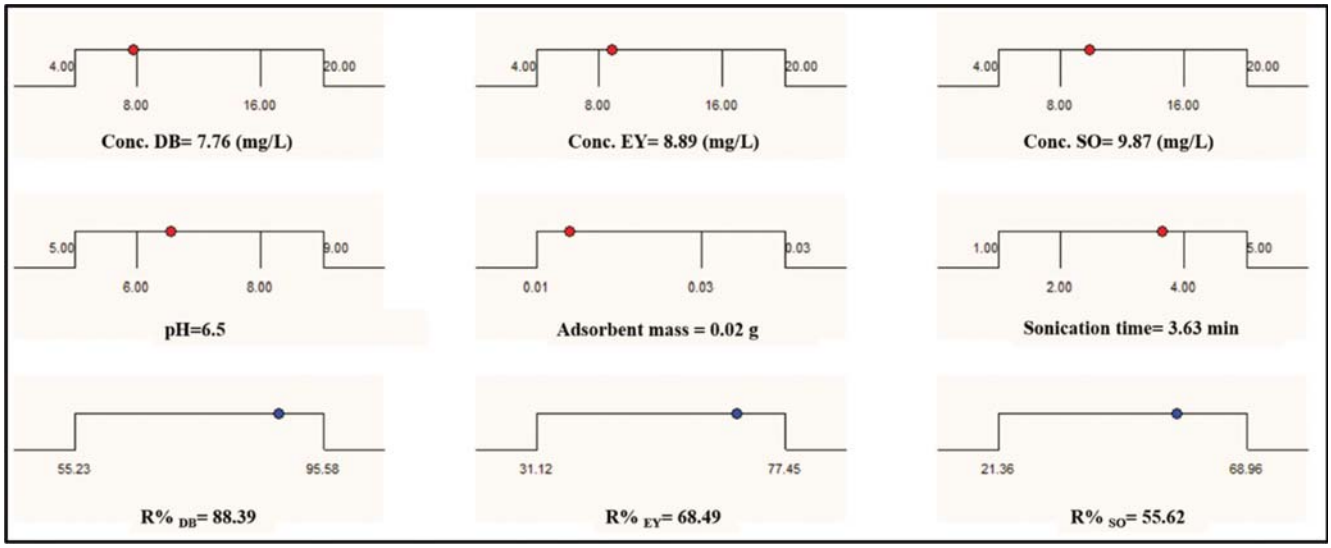

Fig. 7. Profile for predicated values and desirability function for simultaneous removal percentage of selected dyes.

the adsorption percentage. Similar results have been reported in previous studies [20,28].

The effect of CuS-NPs-AC loading on the SO adsorption rate shown in Fig. 6(c) indicates the improved adsorption rate with increasing nanomaterials mass as a result of increased adsorption sites. The results achieved for the influence of the adsorbent dosage for the removal of dyes are in accordance to that described in previous works [31,32].

5. Optimized Conditions

Finding the best operational conditions is important in the adsorption process. We used the desirability function profile subset CCD method to achieve this goal. Results show that the maximum removal efficacies (88.39%, 68.49% and 55.69% for DB, EY and SO, respectively) are achieved at the optimum conditions of 3.63 min of sonication time, 0.02 g of CuS-NPs-AC, 7.76 mg L^{-1} of DB, 8.89 mg L^{-1} of EY, 9.87 mg L^{-1} of SO and pH 6.5 (see Fig. 7). These values reveal that the CuS-NPs-AC even at the lower mass is still able to remove the DB, EY and SO effectively within short sonication time.

6. Adsorption Equilibrium Study

Adsorption isotherm is an empirical relationship used to predict how much solute can be adsorbed by adsorbent and further determine the adsorbent capacity [33,34]. Langmuir, Freundlich isotherms, Dubinin-Radushkevich and Temkin as the simplest known relationships used to describe the adsorption mechanisms and their ability to correlate experimental data is shown in Table 4. Among the linear form of all used adsorption isotherm models, the values of R^2 are more than 0.99 for three dyes in Langmuir adsorption isotherm. Thus, the studied dyes completely adsorbed as monolayer on the CuS-NPs-AC surface and maximum adsorp-

Table 4. Isotherm constant parameters calculated for understudy dyes adsorption onto CuS-NPs-AC

Isotherm	Parameters	Value		
		DB	EY	SO
		0.01 g	0.01 g	0.01 g
Langmuir	Q_m (mg·g^{-1})	198.120	165.0	139.580
	K_a (L mg^{-1})	0.120	0.315	0.520
	R^2	0.998	0.992	0.995
Frendlich	1/n	0.746	0.692	0.623
	K_F (L mg^{-1})	4.120	5.852	5.262
	R^2	0.942	0.902	0.945
Temkin	B_1	31.589	32.189	29.658
	K_T (L mg^{-1})	3.122	4.982	3.692
	R^2	0.971	0.963	0.922
Dubinin-Radushkevich	Q_s (mg g^{-1})	73.690	81.260	75.630
	$B\times10^{-7}$	−2	−1	−1
	E	4545.440	2272.720	2272.720
	R^2	0.935	0.946	0.955

Table 5. Kinetic parameters for the adsorption of understudy dyes onto CuS-NPs-AC

Model	Parameters	Value		
		DB	EY	SO
Pseudo-first-order kinetic	k_1 (min^{-1})	0.596	0.312	1.260
	q_e (calc) (mg g^{-1})	9.250	6.530	5.190
	R^2	0.848	0.912	0.931
Pseudo-second-order kinetic	k_2 (min^{-1})	0.112	0.136	0.259
	q_e (calc) (mg g^{-1})	12.290	11.260	9.630
	R^2	0.992	0.993	0.999
Intraparticle diffusion	K_{diff} (mg g^{-1} $min^{-1/2}$)	4.250	2.890	1.750
	C (mg g^{-1})	5.630	4.520	4.860
	R^2	0.962	0.982	0.952
Elovich	β (g mg^{-1})	0.485	0.725	1.360
	α (mg g^{-1} min^{-1})	362.920	229.684	212.235
	R^2	0.874	0.935	0.963

tion capacity corresponding to monolayer coverage (Langmuir isotherm) is found to be 198.12, 165.0, 139.58 mg g^{-1} for DB, EY and SO, respectively.

7. Adsorption Kinetic Study

To figure out the mechanism of adsorption, it is necessary to investigate the adsorption kinetic. Several kinetic models, such as the pseudo-first-order, pseudo-second order, Elovich and intraparticle diffusion models, have been used to investigate which of them could provide good fit with the experimental data obtained. The pseudo-first-order kinetic model is given with the following equation [35,36]:

$$\log(q_e - q_t) = \log(q_e) - (k_1/2.303)t \quad (8)$$

where q_e shows the dye amount sorbed at equilibrium (mg g^{-1}), q_t is the dye amount sorbed at any time (mg g^{-1}) and k_1 (min^{-1}) refers to rate constant of the pseudo-first-order adsorption. The plot of $\log(q_e - q_t)$ against t should give a linear relationship for which the slope of the plot equals k_1 (Table 5).

The pseudo-second-order kinetic model equation is given as [37,38]:

$$\frac{t}{q_t} = \frac{1}{k_2 q_e^2} + \frac{t}{q_e} \quad (9)$$

where k_2 represents the rate constant of pseudo-second-order sorption (g mg^{-1} min^{-1}) that could be achieved from the plot of t/q_t versus t (Table 5). The intra-particle diffusion process often found as the rate-limiting step in many batch adsorption processes is used to transport the adsorbate species from the solution bulk into the solid phase. The model as expressed in Eq. (10) is used to investigate the feasibility role of intra-particle diffusion during adsorption processes [39].

$$q_t = k_{id} t^{1/2} + C \quad (10)$$

where k_{id} is the rate constant of intra-particle diffusion (g mg^{-1} $min^{-1/2}$) and C (mg g^{-1}) could be obtain from the plot of q_t against $t^{1/2}$ (Table 5). The simplified and linear form of the Elovich equation is expressed as follows:

$$q_t = \beta \ln(\alpha\beta) + \beta \ln t \quad (11)$$

where α and β are the initial sorption rate (mmol g^{-1} min^{-1}) and the desorption constant (g $mmol^{-1}$). The possibility of the Elovich equation is explored using Eq. (11). Therefore, the constants (α and β) can be calculated from the slope and intercept of the linear plot of q_t against $\ln_t$ (Table 5). The validity of the studied models was verified by the correlation coefficient, R^2. Comparison of the R^2 values for different models suggests that the pseudo-second-order kinetic model is the best, mainly due to its highest R^2 value (R^2=1 for three dyes). Pseudo-second-order kinetic model implies that the predominant process here is chemisorption, which involves a sharing of electrons between the adsorbate and the surface of CuS-NPs-AC.

8. Regeneration Performance and Reuse of CuS-NPs-AC

The regeneration and recycling of adsorbents are considered as an important factor in selecting applicable and cost-effective adsorbent in wastewater treatment system. To reuse adsorbents, desorption experiments were carried out with 0.5 M nitric acid. The results of three repeated applications of adsorbent are shown in Fig. 8. The removal efficiency of dyes on adsorbent is slightly reduced after each cycle of the adsorption-desorption process. Thus, it can

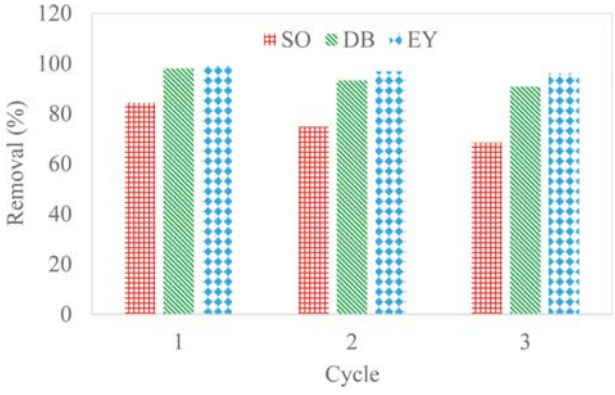

Fig. 8. Reuse of CuS-NPs-AC for the simultaneous adsorption of dyes (C_0=10 mg/L; sonication time=15 min; adsorbent dose= 1.5 g/L).

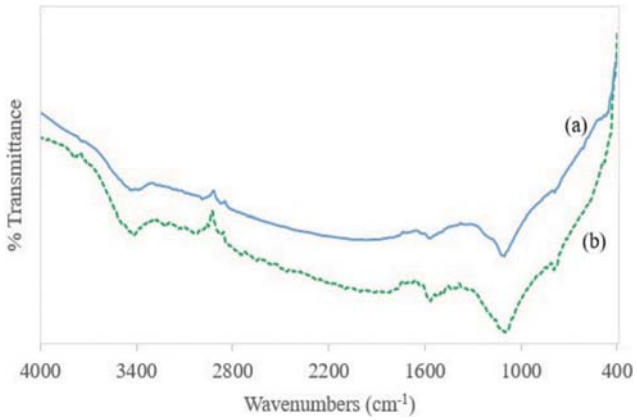

Fig. 9. FTIR spectra of (a) pristine CuS-NPs-AC adsorbent and (b) dyes-loaded CuS-NPs-AC adsorbent.

be said that the as-prepared adsorbent is stable and efficient adsorbent for dyes removal. Fig. 9 shows FTIR spectrum in the range of 400-4,000 cm^{-1}. It is used to specify the functional groups on the CuS-NP-AC. Absorption peak near 3,400 cm^{-1} is probably assigned to the free -OH or NH_2 functional groups. C-H bond vibrations meanwhile cause stretching frequency at 2,900-2,850 cm^{-1}. Characteristic absorption near 1,600 cm^{-1} is attributed to C=O site and strong absorption peak near 1,100 cm^{-1} probably related to C-O stretching frequency. Comparison of the FTIR spectra of both original and dye-loaded adsorbent shows that some functional groups have alterations in their intensity and frequency, which confirms the bonding interactions of the functional groups with the dye molecules [40].

9. Comparison with other Adsorbents

By Langmuir isotherm as best fitted model, the adsorbent capacities were calculated as 198.12, 165.0, 139.58 mg g^{-1} for DB, EY and SO dyes, respectively. Table 6 compares the adsorption capacity of CuS-NPs-AC for DB, EY and SO dyes with other adsorbents reported in the literature. As can be seen, the adsorption capacities of the CuS-NPs-AC for DB, EY and SO dyes are considered promising compared to some of the works that reported the adsorption capacities of less than 100 mg g^{-1}. Although some research works could produce the absorbents with capacities greater than our findings, a conclusion is not easy to make because adsorbent properties and experimental conditions are the two main factors that can lead to differences between adsorption capacities.

CONCLUSION

CuS-NPs-AC was prepared as an adsorbent and used for dye removal. The results showed that the newly synthesized CuS-NPs-AC possessed promising adsorption efficiency with a Langmuir monolayer adsorption capacity of 198.12, 165.0, 139.58 mg g^{-1} for DB, EY and SO, respectively. The adsorption of dyes from aqueous medium onto the CuS-NPs-AC fitted well with the pseudo-second-order kinetic model, confirming its good correlation with the experimental data. The synthesized CuS-NPs-AC also showed promising performance for simultaneous adsorption of three different types of dyes (DB, EY and SO) from aqueous solution.

ACKNOWLEDGEMENTS

The authors would like to thank the Research Council of the Islamic Azad University of Gachsaran branch, Iran, for financially supporting this work.

REFERENCES

1. N. Cheng, Q. Hu, Y. Guo, Y. Wang and L. Yu, *ACS Appl. Mater.*

Table 6. Comparison of adsorption capacity of CuS-NPs-AC for DB, EY and SO dyes with different types of adsorbents

Adsorbent	Dye	Adsorption capacity (mg/g)	Reference
CuS-NP-AC	DB	243.90	[19]
Cu@IL-ONO	EY	286.00	[41]
Ag-NP-AC	EY	250.00	[41]
Carbon prepared from tea waste	EY	400.00	[42]
Nano-sized chitosan blended polyvinyl alcohol	EY	52.91	[43]
Teak leaf litter powder	EY	31.64	[44]
γ-Al_2O_3	EY	47.78	[45]
Graphene oxide nanosheets	EY	217.33	[46]
Fe_3O_4 modified with sodium dodecyl sulfate	SO	769.23	[47]
Fe_3O_4 nanoparticles	SO	91.90	[48]
ZnO-NR-AC	SO	55.25	[49]
CO_2 neutralized activated red mud waste	SO	9.77	[50]
NaOH-treated sugarcane bagasse	SO	62.88	[51]
Modified red mud	SO	89.40	[52]
AC derived from Peltophorum Pterocarpum	SO	221.91	[53]
CuS-NP-AC	DB	198.12	This work
CuS-NP-AC	EY	165.00	This work
CuS-NP-AC	SO	139.58	This work

Interfaces, **7**, 10258 (2015).
2. T. Madrakian, A. Afkhami, M. Ahmadi and H. Bagheri, *J. Hazard. Mater.*, **196**, 109 (2011).
3. X. Zhu, Y. Liu, C. Zhou, S. Zhang and J. Chen, *ACS Sustainable Chem. Eng.*, **2**, 969 (2014).
4. E. Forgacs, T. Cserhati and G. Oros, *Environ. Int.*, **30**, 953 (2004).
5. M. Asgher and H. N. Bhatti, *Ecological Engineering*, **38**, 79 (2012).
6. V. K. Gupta, I. Ali, T. A. Saleh, A. Nayak and S. Agarwal, *Rsc Adv.*, **2**, 6380 (2012).
7. T. A. Saleh and V. K. Gupta, *J. Colloid Interface Sci.*, **371**, 101 (2012).
8. A. K. Verma, R. R. Dash and P. Bhunia, *J. Environ. Manage.*, **93**, 154 (2012).
9. V. K. Gupta, R. Kumar, A. Nayak, T. A. Saleh and M. Barakat, *Adv. Colloid Interface Sci.*, **193**, 24 (2013).
10. T. A. Saleh, A. M. Muhammad and S. A. Ali, *J. Colloid Interface Sci.*, **468**, 324 (2016).
11. M. Gonçalves, M. C. Guerreiro, L. C. A. de Oliveira and C. S. de Castro, *J. Environ. Manage.*, **127**, 206 (2013).
12. T. A. Saleh, *Desalination Water Treatment*, **57**, 10730 (2016).
13. M. Ghaedi, M. Yousefi-Nejad, M. Safarpoor, H. Z. Khafri, I. Tyagi, S. Agarwal and V. K. Gupta, *Desalination Water Treatment*, **57**, 24456 (2016).
14. M. Ghaedi, A. Ansari, F. Bahari, A. Ghaedi and A. Vafaei, *Spectrochim. Acta Part A: Mole. Biomolecular Spectroscopy*, **137**, 1004 (2015).
15. M. Roosta, M. Ghaedi, A. Daneshfar and R. Sahraei, *Spectrochim. Acta Part A: Mole. Biomolecular Spectroscopy*, **122**, 223 (2014).
16. M. Khajeh and M. Gharan, *J. Chemometrics*, **28**, 539 (2014).
17. T. Nazghelichi, M. Aghbashlo and M. H. Kianmehr, *Comput. Electronics Agriculture*, **75**, 84 (2011).
18. M. Ghaedi, S. Khodadoust, H. Sadeghi, M. A. Khodadoust, R. Armand and A. Fatehi, *Spectrochim. Acta Part A: Mol. Biomolecular Spectroscopy*, **136**, 1069 (2015).
19. A. R. Bagheri, M. Ghaedi, A. Asfaram, S. Hajati, A. M. Ghaedi, A. Bazrafshan and M. R. Rahimi, *J. Taiwan Inst. Chem. Engineers*, **65**, 212 (2016).
20. A. R. Bagheri, M. Ghaedi, S. Hajati, A. M. Ghaedi, A. Goudarzi and A. Asfaram, *RSC Adv.*, **5**, 59335 (2015).
21. M. Ghaedi, K. Dashtian, A. M. Ghaedi and N. Dehghanian, *Physical Chemistry Chemical Physics*, **18**, 13310 (2016).
22. F. N. Azad, M. Ghaedi, K. Dashtian, S. Hajati and V. Pezeshkpour, *Ultrasonics Sonochemistry*, **31**, 383 (2016).
23. S. Dashamiri, M. Ghaedi, K. Dashtian, M. R. Rahimi, A. Goudarzi and R. Jannesar, *Ultrasonics Sonochemistry*, **31**, 546 (2016).
24. S. Mosleh, M. R. Rahimi, M. Ghaedi and K. Dashtian, *Ultrasonics Sonochemistry*, **32**, 387 (2016).
25. M. Soleiman, M. R. Rahimi, M. Ghaedi, K. Dashtian and S. Hajati, *RSC Adv.*, **6**, 17204 (2016).
26. S. Hosseini, M. A. Khan, M. R. Malekbala, W. Cheah and T. S. Choong, *Chem. Eng. J.*, **171**, 1124 (2011).
27. T. A. Saleh and V. K. Gupta, *Nanomaterial and polymer membranes: Synthesis, characterization, and applications*, Elsevier (2016).
28. M. Ghaedi, A. M. Ghaedi, F. Abdi, M. Roosta, R. Sahraei and A. Daneshfar, *J. Ind. Eng. Chem.*, **20**, 787 (2014).
29. G. B. Celli, A. Ghanem and M. S.-L. Brooks, *Ultrasonics Sonochemistry*, **27**, 449 (2015).
30. T. A. Saleh, M. Tuzen and A. Sarı, *Chem. Eng. Res. Design*, **117**, 218 (2017).
31. S. O. Adio, M. H. Omar, M. Asif and T. A. Saleh, *Process Safety Environ. Protection*, **107**, 518 (2017).
32. T. A. Saleh, A. Sarı and M. Tuzen, *J. Environ. Chem. Eng.*, **5**, 1079 (2017).
33. Y.-S. Ho, *Polish J. Environ. Studies*, **15**, 81 (2006).
34. Y.-S. Ho, *Carbon*, **42**, 2115 (2004).
35. Y. S. Ho and G. McKay, *Chem. Eng. J.*, **70**, 115 (1998).
36. S. Lagergren, *Kungliga Svenska Vetenskapsakademiens. Handlingar*, **24**, 1 (1898).
37. Y.-S. Ho, *Water Res.*, **40**, 119 (2006).
38. Y.-S. Ho and G. McKay, *Process Biochem.*, **34**, 451 (1999).
39. W. J. Weber and J. C. Morris, *J. Sanitary Engineering Division*, **89**, 31 (1963).
40. T. A. Saleh, S. Agarwal and V. K. Gupta, *Appl. Catal. B: Environ.*, **106**, 46 (2011).
41. M. Ravanan, M. Ghaedi, A. Ansari, F. Taghizadeh and D. Elhamifar, *Spectrochim. Acta Part A, Mol. Biomolecular Spectroscopy*, **123**, 467 (2014).
42. L. Borah, M. Goswami and P. Phukan, *J. Environ. Chem. Eng.*, **3**, 1018 (2015).
43. T. Anitha and S. Kumar, *J. Water Process Eng.*, **13**, 127 (2016).
44. E. O. Oyelude, J. A. Awudza and S. K. Twumasi, *Scientific Reports*, **7**, 12198 (2017).
45. M. S. Thabet and A. M. Ismaiel, *J. Encapsulation Adsorption Sci.*, **6**, 70 (2016).
46. P. Veerakumar, J. Tharini, M. Ramakrishnan, I. Panneer Muthuselvam and K. C. Lin, *ChemistrySelect*, **2**, 3598 (2017).
47. S. Shariati, M. Faraji, Y. Yamini and A. A. Rajabi, *Desalination*, **270**, 160 (2011).
48. M. Ghaedi, S. Hajjati, Z. Mahmudi, I. Tyagi, S. Agarwal, A. Maity and V. K. Gupta, *Chem. Eng. J.*, **268**, 28 (2015).
49. F. N. Azad, M. Ghaedi, K. Dashtian, S. Hajati, A. Goudarzi and M. *New J. Chem.*, **39**, 7998 (2015).
50. M. K. Sahu, U. K. Sahu and R. K. Patel, *RSC Adv.*, **5**, 42294 (2015).
51. M. Farahani, M. Kashisaz and S. Abdullah, *Int. J. Ecol. Sci. Environ. Eng.*, **2**, 17 (2015).
52. M. K. Sahu and R. K. Patel, *RSC Adv.*, **5**, 78491 (2015).
53. Y. Subbareddy, C. Jayakumar, S. Valliammai, K. Nagaraja and B. Jeyaraj, *Desalination Water Treatment*, **55**, 1048 (2015).